THE JOURNAL OF PHYSICAL CHEMISTRY C
A JOURNAL OF THE AMERICAN CHEMICAL SOCIETY

pubs.acs.org/JPCC

Article

Assigning Optical Absorption Transitions with Light-Induced Crystal Structures: Case Study of a Single-Crystal Nanooptomechanical Transducer

Jacqueline M. Cole,* David J. Gosztola, Sven O. Sylvester, SuYin Grass Wang, and Yu-Sheng Chen

Cite This: *J. Phys. Chem. C* 2021, 125, 15711−15723

Read Online

ACCESS | Metrics & More | Article Recommendations | Supporting Information

ABSTRACT: UV/vis absorption spectroscopy affords indirect structural information about the photochemistry and photophysics of molecules by inferring types of electronic transitions from spectral features. Direct structural information would become available, though, if light-induced crystal structures could be mapped against changes in optical absorption spectra as a photochemical process evolves. We present a series of light-induced crystal structures that track real-time changes in solid-state optical absorption spectra of a crystalline nanooptomechanical transducer, while the transduction process unfolds within its crystal lattice at 100 K. Results afford a combined structural and spectral mapping of its solid-state optical absorption, from which the operational mechanism of nanooptomechanical transduction is revealed. Metal-to-ligand and metal-centered charge-transfer bands are assigned to optical absorption peaks directly from their three-dimensional (3D) light-induced crystal structures. This approach could be used to characterize many solid-state optoelectronic materials.

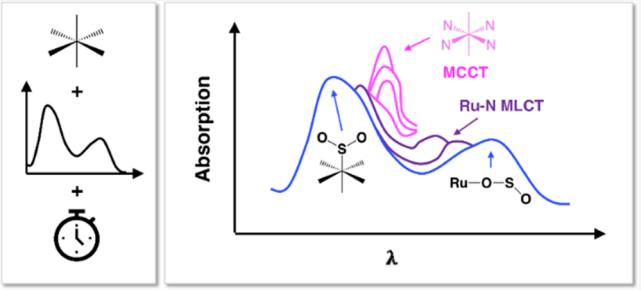

INTRODUCTION

UV/vis absorption spectroscopy is ubiquitous in photochemistry and photophysics, owing to its role as a core materials characterization method to verify a new synthetic product or to elucidate photoinduced effects in advanced optical materials. Spectral features of a given chemical are assigned to electronic transitions that are characteristic of its optically absorbing molecular constituents. These assignments are generally made using one of two characterization options: (1) empirical knowledge from *a priori* assignments of related materials with the functional group beacons and (2) theoretical calculations that simulate optical absorption spectral features of a molecule in its gas or solution phase using time-dependent density functional theory. There is no generic classification table for UV/vis absorption spectra, unlike other materials characterization techniques, such as nuclear magnetic resonance (NMR) or vibrational spectroscopy (infrared or Raman), since changes are too subtle and material-specific to be generalized.

The characterization of optical absorption spectra is predominantly carried out in the solution phase. The acquisition of solid-state spectra is more difficult, especially in single crystals on account of their small sizes. Meanwhile, calculations offer limited help to characterize them because simulations of solid-state optical absorption are very challenging,[1] especially for organometallic compounds. Yet, such spectra typically reveal the intramolecular charge-transfer (ICT) characteristics of a chemical, knowledge of which is key to determining the viability of advanced optical materials for many types of solid-state device technologies. Nonetheless, UV/vis absorption spectra tend to yield only indirect and qualitative ICT information.

Technical developments in *in situ* light-induced single-crystal X-ray diffraction (now known as photocrystallography)[2−6] have come some way to help meet this need. This technique characterizes the crystal structure of a chemical while in its light-induced state, as has now been demonstrated for a broad range of compounds.[7−32] Photocrystallography can therefore determine light-induced changes in the electronic structure of a compound, which are afforded by ICT transitions. This photostructural information is direct and quantitative. For example, ICT transitions such as metal-to-ligand charge transfer (MLCT) would manifest as photoinduced bond-length changes in metal and ligand coordination. However, photocrystallography does not provide information about energies that are associated with ICT transitions. Both the structural and energetic nature of ICT characteristics are

Received: May 19, 2021
Revised: June 14, 2021
Published: July 9, 2021

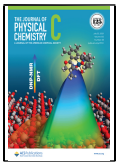

Scheme 1. (A) Linkage Photoisomerization Process. (B) Basic Two-Step Structural Mechanism for Nanooptomechanical Transduction, Assumed for 1 Based on Previous Work on Related Complexes[22]

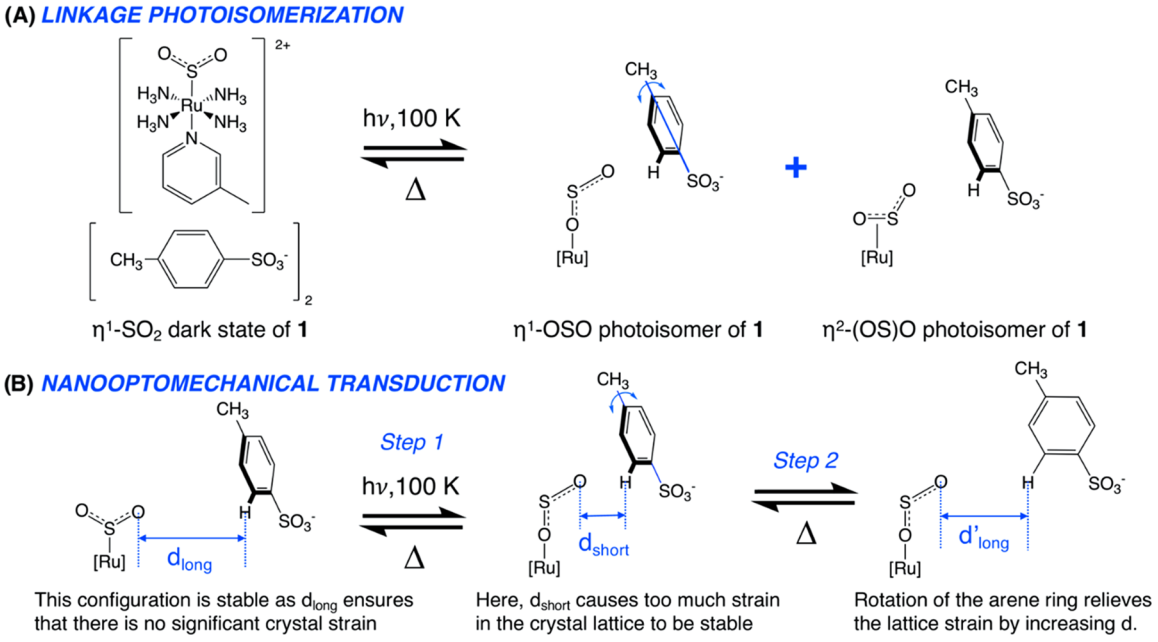

important for exploring potential applications of advanced optical materials. Thus, we ideally need a metrological approach that provides correlated structural and energetic information about ICT transitions in the solid state.

We recently showcased a metrological approach that offers correlated single-crystal optical absorption spectroscopy and photocrystallography.[7] This approach was designed for exploring the structure and function of single-crystal optical actuators. Such materials belong to an emerging research field of chemistry, given their attractive solid-state switching and transduction capabilities.[33−37] Prospective applications range from optical sensing,[38] to photocatalysis,[39] to light-induced molecular machines,[40] to futuristic circuitry for quantum computers.[41] This metrological approach could be extended to perform experiments via a time sequence of measurements. One could then ascertain how ICT alters the structure and optical absorption of a crystalline compound as it is exposed to light for time, *t*.

This paper demonstrates such an approach, allowing charge-transfer bands in single-crystal optical absorption spectra to be characterized directly by light-induced crystal structures. Thereby, a time sequence of correlated photocrystallographic and single-crystal optical absorption spectroscopic experiments is performed as a function of light-exposure time on a crystalline material. While this approach is eminently transferable to any light-responsive crystalline material, a type of single-crystal optical actuator that undergoes nanooptomechanical transduction was selected as a case study. A chemical is a nanooptomechanical transducer if it undergoes a light-driven switching process in which one molecule or ion stimulates mechanical motion in a neighboring molecule or ion. Materials that exhibit this phenomenon in their single-crystal form are of particular interest since they offer a high-quality solid-state medium for single-photon control. They also carry long-range effects throughout the material, given the periodic nature of a crystal-lattice environment. This can lead to correlated photoswitching behavior, whose "out-of-equilibrium" effects have been coined as "the real *terra nova* of solid-state chemistry".[42] Our choice of case study therefore prospects a demonstration of ICT characterization from evolving photostructural and optical absorption spectral data. Our findings will show that such data reveal new insights into the detailed operational mechanism of nanooptomechanical transduction in a new compound, *trans*-[Ru(SO$_2$)(NH$_3$)$_4$(3-methylpyridine)]tosylate$_2$ (**1**).

1 belongs to a series of complexes based on the generic formula, *trans*-[Ru(SO$_2$)(NH$_3$)$_4$X]$^{m+}$Y$_n$, whose ligand, X, lies *trans* to the SO$_2$ group, which manifests solid-state linkage photoisomerization, while Y is a counterion; *m* and *n* are integers that simply depict charge-balancing requirements, depending on the nature of X and Y.[7,19−32,43,44] Only certain combinations of X and Y will afford nanooptomechanical transduction, the first example of which was reported by Sylvester and Cole.[22] They used photocrystallography[2−6] to deduce a basic two-step mechanistic understanding of its nanooptomechanical transduction. The first step entails the photoisomerization of an S-bound η^1-SO$_2$ ligand to an O-bound η^1-OSO photoisomer with the concomitant formation of a minor side-bound η^2-(OS)O species. One oxygen in the η^1-OSO photoisomer protrudes from the ruthenium-based cation such that it is so close to one of its neighboring tosylate anions that it imparts crystal-lattice strain. The arene ring of this tosylate ion rotates to alleviate the strain; this is the second (transduction) step of the mechanism (see Scheme 1). The structural information afforded by that study was limited to that acquired before and after light irradiation. This was sufficient to discover a few other material examples of this phenomenon in this family of complexes.[23−25] However, more detailed mechanistic information about the nanooptomechanical transduction process was lacking. In particular, structure−property relationships could not be unraveled, even though they are likely to be correlated to its operational mechanism. We now present results that uncover such relationships in **1**; specifically, we show how correlated metal-based charge

https://doi.org/10.1021/acs.jpcc.1c04425
J. Phys. Chem. C 2021, 125, 15711−15723

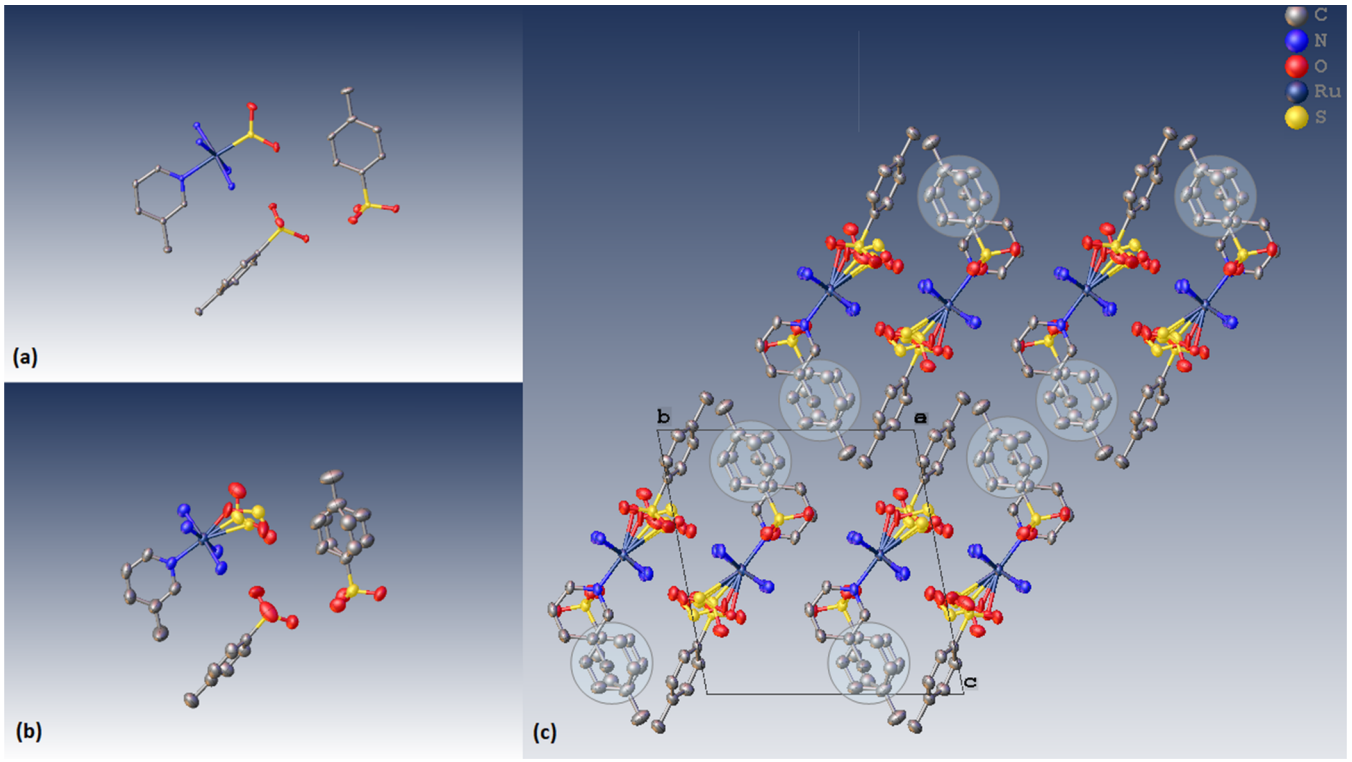

Figure 1. (a) Dark-state and (b) light-induced crystal structure of **1**. (c) Crystal packing of **1** looking down the crystallographic *a* axis. The carbon atom of the methyl group in the 3-methylpyridine ligand librates primarily in a direction that points directly into each disordered arene ring in the crystal lattice, as highlighted by its anisotropic displacement parameter (ADP) that lies centrally above or below these rings in the encircled regions. All structures were visualized using OLEX2.[45]

transfer and photostructural changes are responsible for the mechanistic function of **1**.

MATERIALS AND METHODS

Photostructural and Optical Characterization of 1 in Its Single-Crystal Form. Single crystals of **1** precipitated from solution during its synthesis (see the Supporting Information). Dark-state and light-induced structures of **1** were characterized by photocrystallography;[2−6] see the Supporting Information. The photocrystallography results afforded a series of light-induced crystal structures of **1** as a function of the total time, t, that the crystal was exposed to 505 nm light at 100 K. Thereby, 12 and 24 light-induced crystal structures of **1** were determined from two time sequences of photocrystallographic data that were acquired from a crystal of size 0.05 × 0.03 × 0.01 mm^3 (crystal I) or 0.17 × 0.09 × 0.01 mm^3 (crystal II), which were exposed to light for up to t = 2 or 121 min, respectively; see Figures 1 and 2 and Movies S1 and S2 in the Supporting Information. The longer time sequence of photocrystallographic data was complemented by a time-matched sequence of single-crystal optical absorption spectra of **1** that were also acquired on crystal II (see Figure 3), using a custom-built microspectroscopy system; for technical details, see the Supporting Information and Cole et al.[7] Photocrystallographic data were additionally collected for one longer light-exposure time, t = 181 min, to yield a light-induced crystal structure whose role was simply to confirm that the extent of photoisomerization had completed as far as this was possible. Note that the SO_2 isomer cannot fully photoisomerize in **1**, as is typical for this family of [$RuSO_2$] complexes, owing to crystal-lattice strain that builds up during the photoisomerization process.[4] The limit by which species in **1** can photoconvert is such that its dark-state S-bound η^1-SO_2 isomer remains the predominant species once **1** has maximally photoisomerized (see Figure 3).

The photosensitive species in **1** consist of (i) the SO_2 isomer, which photoisomerizes to the O-bound η^1-OSO and the side-bound η^2-(OS)O configuration, (ii) the arene ring of one of the tosylate ions that forms a light-induced rotor (hereafter known as the rotor), and (iii) the anisotropic displacement parameter (ADP) of the carbon atom (C6) in the methyl group of the 3-methylpyridine ligand, which librates increasingly as a function of light-exposure time; this libration occurs primarily along a trajectory that lies perpendicular to the pyridine ring, as denoted by the first-principal second-rank tensor, U_{11}, of the ADP of C6.

It is worth noting that no isosbestic points are present in our single-crystal optical absorption spectra. This suggests that strong deviations from linear absorption occur when measuring optical absorption spectra of **1** in their single-crystal form because the presence of an isosbestic point is reliant upon the Beer−Lambert law holding. Indeed, none of our studies that report single-crystal optical absorption spectra so far[7,24−26,29,32] have evidenced the presence of any isosbestic points. The crystals used in those studies were judged to exhibit a significant amount of nonlinear absorption, based on our empirical findings, whereby we could characterize bulk photoisomerization in crystals that were substantially thicker than what is possible from a simple calculation of optical absorbance from the Beer−Lambert law. Non-Beer−Lambert behavior has been observed when measuring various solid-state media, including particulate suspensions,[46] and glassy and nematic elastomers that bend upon the application of light.[47,48]

https://doi.org/10.1021/acs.jpcc.1c04425
J. Phys. Chem. C 2021, 125, 15711−15723

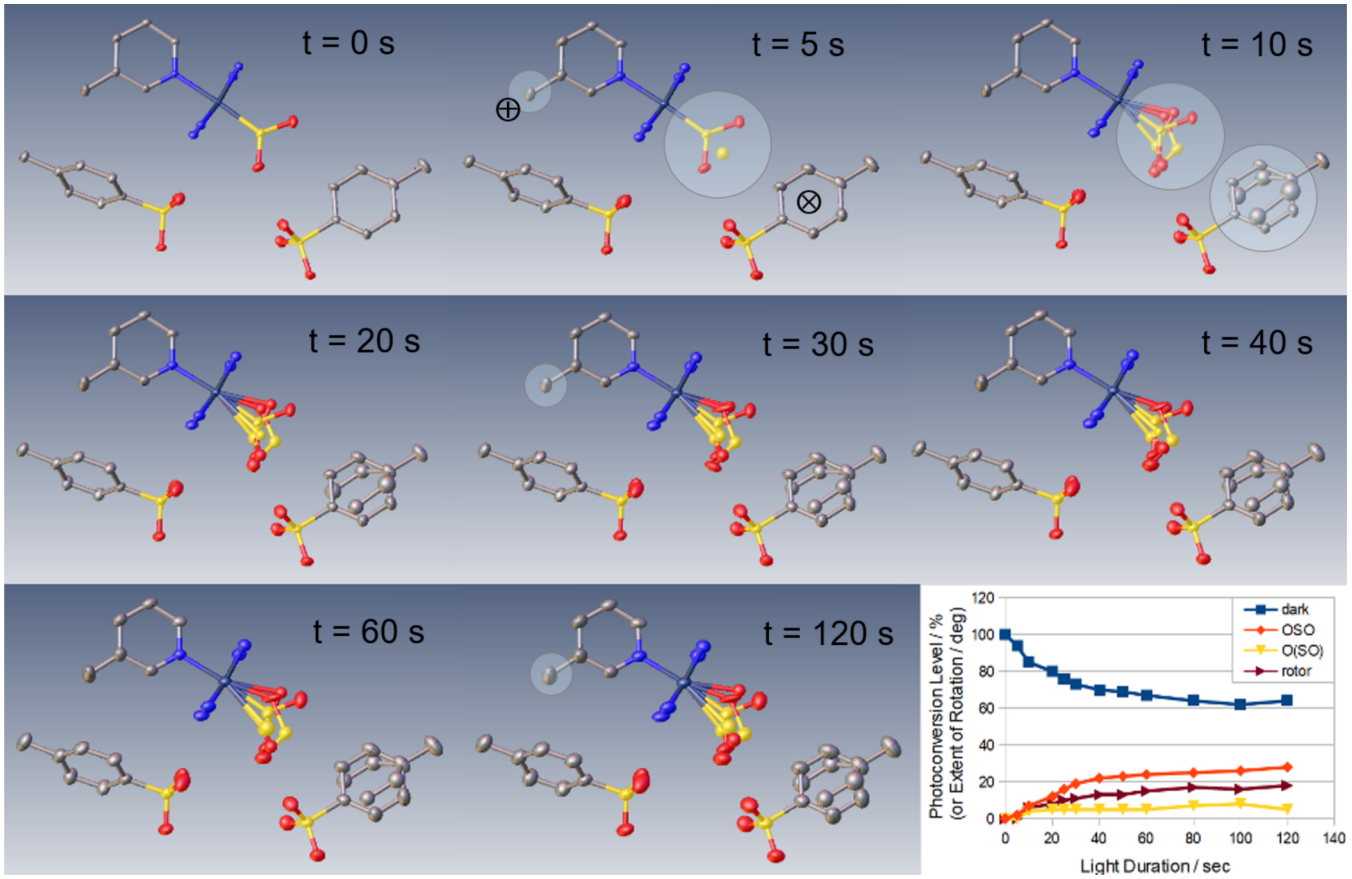

Figure 2. Eight crystal structures of **1** (crystal I) realized as a function of t seconds of a 505 nm light exposure from t = 0 to 120 s. The heaviest element of the light-induced η^1-OSO ligand (sulfur) can already be refined after 5 s of light exposure. The anisotropic displacement parameter (ADP) of the carbon atom (C6) in the methyl substituent of the 3-methylpyridine ligand also starts to become more elongated at t = 5 s, *i.e.*, C6 exhibits libration and this continues to grow throughout this entire time sequence (see the small circled highlights). C6 librates in the direction that points into the center of the arene ring of the ring rotor, within the periodic framework of the crystal lattice (the trajectory lies perpendicular to the page, as shown by the head (⊕) and tail (⊗) ends of an arrow). By t = 10 s, this arene ring has started to rotate as a consequence of this interaction with C6 as well as its proximity to the protruding oxygen of the η^1-OSO photoisomer, enough of which has now formed that it can be distinguished and refined crystallographically (see the large circled highlights). The plot in the bottom-right panel shows that the photoconversion levels of the rotated ring and both photoisomers (a small amount of η^2-(OS)O is also refined) continue to grow with time, while that of the dark-state η^1-SO_2 configuration decreases. The changing gradients in this plot indicate that three distinct mechanistic steps occur as a function of a 505 nm light exposure to **1** in crystal I, in the regions t = 0−5, 10−40, and 50−120 s. Movie S1 in the Supporting Information displays all 12 crystal structures of **1** (crystal I) in this time-sequenced series together with a dynamic view of the changing photoconversion levels of each light-sensitive structural constituent of **1** and its single-crystal optical absorption spectra at 1 min intervals. All structures were visualized using OLEX2.[45]

Isosbestic points may also be precluded where solvatochromism occurs for some reason. This includes certain linkage photoisomerization studies, where the lack of isosbestic points, despite successful photoconversion, has been addressed explicitly.[49] We also observe solvatochromism in this and our related studies.[7,24−26,29,32]

■ RESULTS AND DISCUSSION

The correlated photostructural and optical absorption spectroscopy results are shown in Movies S1 and S2 for crystals I and II, respectively, as well as being visualized as time sequences in Figures 2 and 3. Their correlated presentation permits structural and optical property changes in **1** to be considered collectively by direct observation.

Observations from the Molecular Movies. The light-induced crystal structure of **1** shows evidence of η^1-OSO photoisomerization after just 5 s of light exposure, whereby it was already possible to refine its heaviest (sulfur) atom (*cf.* highlighted SO_2 region, top, middle panel, Figure 2). By this point, the libration in C6 has also started to increase in the U_{11} direction, *i.e.*, perpendicular to the plane of the pyridine ring.

Data acquired on **1** during 10−40 s of light exposure (Figure 2, bottom right) shows that the rate by which the dark-state SO_2 isomeric fraction depletes has now dropped, while the largest rate increase displayed in Figure 2 is associated with η^1-OSO formation; the latter thus drives the photoisomerization process within this time regime. All atoms of both η^1-OSO and η^2-(OS)O photoisomers can be refined in a crystal structure once **1** has been subjected to at least 10 s of light (*cf.* highlighted SO_2 region, top, right panel, Figure 2). The arene ring in one of the tosylate ions (the rotor) also displays a rotational disorder by this point (*cf.* highlighted arene, top, right, Figure 2). All ADPs for the η^1-OSO ligand can be refined in crystal structures that have been exposed to at least 25 s light, while nearly 20% of the SO_2 ligands have photoconverted to the η^1-OSO configuration by 30 s of light. The extent of photoconversion in the rotor tracks that of the η^1-OSO ligand, although its level lags by ca. 10% throughout the light-exposure

https://doi.org/10.1021/acs.jpcc.1c04425
J. Phys. Chem. C 2021, 125, 15711−15723

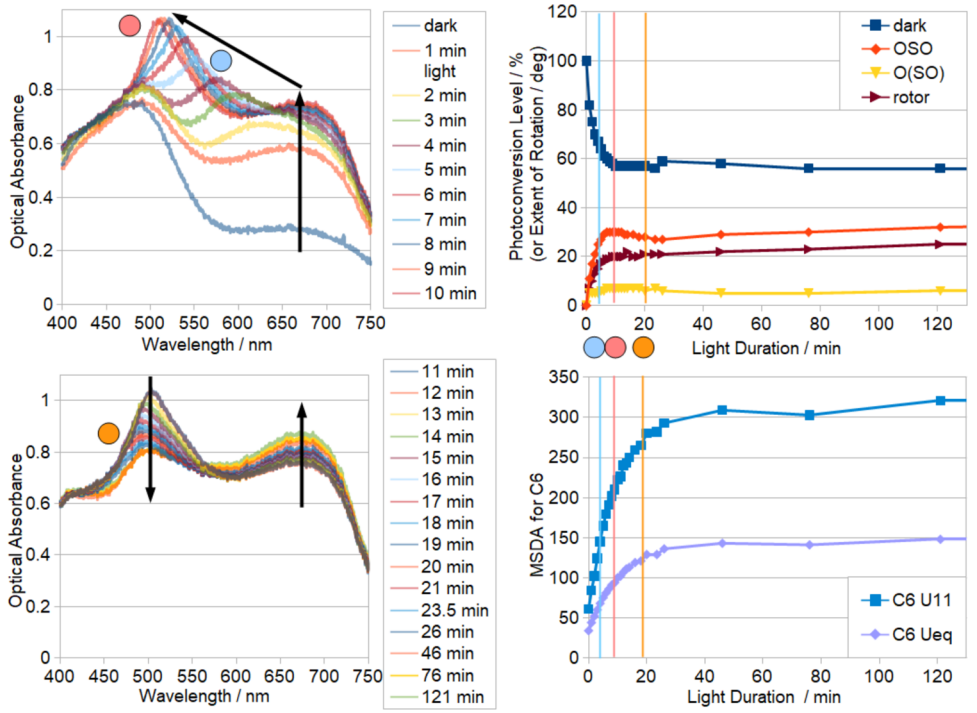

Figure 3. (Left) Single-crystal optical absorption spectra of **1** (crystal I) as a function of t min of a 505 nm light exposure; (right, top) fractional occupancy of the η^1-SO_2, η^1-OSO, and η^2-(OS)O ligands and the ring rotor of **1** as a function of t min of a 505 nm light exposure; the arrows indicate the trajectories of changing optical absorption. (Right, bottom) Mean-square displacement amplitude (MSDA) of the carbon atom (C6) in the methyl group of the pyridyl ring of **1** as a function of t mins of a 505 nm light exposure (U_{11} and U_{eq} are the principal components, 11, and the equivalent isotropic MSDA $(U_{11} + U_{22} + U_{33})/3$, respectively). The circle and line annotations relate the optical absorption and crystal structure parameters of **1** at key time points: (cyan) t = 5 min, beyond which solvatochromatic effects appear to ensue; (pink) t = 10 min, when the optical absorption and fractional occupancy of the η^1-OSO and ring rotor all reach maxima; (orange) t = 20 min, beyond which the fractional occupancies of all SO_2 ligand configurations, the ring rotor, and the MSDA of C6 change little, while the optical absorption decreases and increases in the blue and red regions of the visible spectrum.

process. η^2-(OS)O photoisomer formation is not favorable given that it barely exceeds a 5% photoconversion at any point in the light-exposure process. Besides, it is the η^1-OSO photoisomer that engenders the rotation of the arene ring in a tosylate ion to form the rotor, *i.e.*, nanooptomechanical transduction.

The crystal absorbs light mostly in the 550−750 nm region during the first minute of light exposure, with the optical absorbance of **1** doubling at the wavelength of largest change (650 nm). The waveband associated with this peak at 650 nm starts to undergo a hypsochromic shift in optical absorption between 1 and 2 min of light exposure (Movie S1). This process takes on another distinctive form within this time frame, as is evidenced via Figure 2 (bottom right); indeed, the photoconversion fractions of all photosensitive structural constituents of **1** are now essentially comparable by this stage of the photoisomerization process.

The rates at which each photoconverted species change converge during the t = 2−5 min regime (see Figure 3, top right). This suggests that the photosensitive species start to operate via a single contiguous mechanism beyond t = 5 min. In turn, this suggests that the onset of a further change in the operational mechanism occurs. During the light-exposure time period, 5 min < t < 10 min, the lower-wavelength absorption peak (ca. 500 nm) becomes essentially constant, while the other peak continues its hypsochromic shifting until its wavelength starts to reach that of the lower-wavelength peak after c. 10 min light exposure. The peak has become relatively narrow by this point, while its optical absorbance has reached its maximum value of just over 1.0. The photoconversion levels of the SO_2 ligand and the arene-ring rotor have started to level out by this point. Further light exposure to **1** extends the hypsochromic shifting, while its peak absorbance begins to diminish. Eventually, the band stops shifting, at which point the two original peaks in the optical absorption spectrum appear to have coalesced. The optical-absorption shoulder whose peak lies at ca. 675 nm then increases between 20 and 120 min, during which time the photoconversion levels and U_{11} of C6 display a marginal monotonic change as they tend to constant values. There is a small absorption dip at ca. 450 nm after ca. 40 min light exposure, but otherwise, little changes after 20 min light exposure. All atoms appear to absorb light as heat after 40 min, judging from their significant increase in ADP values during this time period. However, there is a particularly marked increase in the ADPs for the oxygens of the dark-state configuration of SO_2, and this occurs with a concomitant increase in long-wavelength absorption. The photoconversion level of the η^2-(OS)O configuration increases and then diminishes slightly during this time. Overall, these molecular movies indicate that there are five discrete light-exposure time periods that define distinct steps of the operational mechanism for nanooptomechanical transduction in **1**. These are summarized in Figure 4.

Assigning Light-Induced Metal-Based Charge-Transfer Characteristics in 1 from Bond-Length Changes. We now relate these changes in optical absorption to those of the structure more quantitatively by comparing bond-length changes in **1** with those of optical absorption spectra as a

https://doi.org/10.1021/acs.jpcc.1c04425
J. Phys. Chem. C 2021, 125, 15711−15723

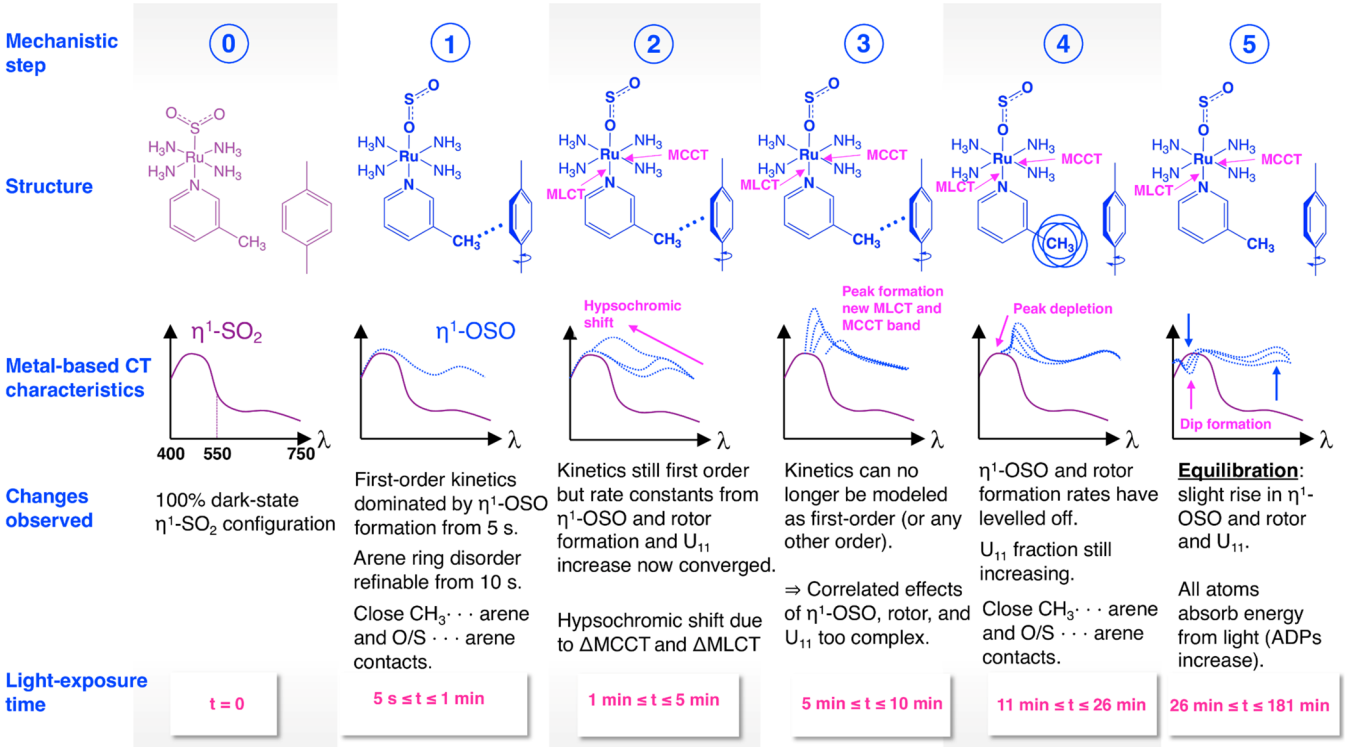

Figure 4. Summary of the five discrete steps of the operational mechanism for nanooptomechanical transduction in **1**, as determined by this study. The displayed formation of the η^1-OSO photoisomer is accompanied by a small amount of the side-bound η^2-(OS)O photoisomer and a residual dark-state η^1-SO_2 configuration, which is the dominant species. However, these are not shown for the purposes of clarity. Likewise, the light-induced steps in this figure display only the rotated arene ring even though they do not occur in all unit cells.

function of light-exposure time. Figures 5 and S8−S13 present these bond-length changes that have been partitioned into distinct parts of the cations and anions for **1**. One cannot partition the spectral contributions from these distinct parts of the complex in a similarly explicit manner. However, the time-sequenced series of changes in these spectra as a function of light duration time do expose the contributions of individual parts of the complex, as their features generally dominate at different time points. This is a key asset of our approach as it affords an ability to make spectroscopic assignments about individual components of a complex from those of their structure, as well as considering the structure and optical absorption spectral characteristics overall. The core tenet of the spectroscopic assignment process relies on forging structure−spectra relationships from empirical observations, via the following sequential workflow: (a) empirically deduce structure−spectra relationship(s) at specific time points where distinct changes in the structure and spectra are observed to occur; (b) where possible, rationalize these correlated structural and spectral changes at a given time point by considering how these metrological features may be related chemically; (c) where relevant, use previous spectroscopic assignments from the literature on reference compounds to label or corroborate the spectral features for which the empirical relationships have been deduced via (a) and (b). Overall, this strategy permits the five distinct optical absorption features in **1** shown in Figure 4 to be assigned to metal-based charge-transfer characteristics directly from crystal structure information.

The ruthenium coordination environment is associated with, by far, the largest bond-length changes that occur in **1** within the first minute of light exposure (step 1, Figure 4). This stands to reason given we saw earlier that the η^1-OSO photoisomer in **1** starts to form during this period. All bonds in the ruthenium core respond to this onset of photoisomerization. In particular, the Ru−S coordination strength of the residual dark-state η^1-SO_2 configuration increases markedly (Figure 5 (top left)) to compensate for the weaker nature of the Ru−O bond from the η^1-OSO photoisomer[50] that forms at the direct expense of some of the η^1-SO_2 species. A large *trans* influence is also observed, whereby the Ru−$N_{pyridyl}$ coordination strength increases substantially (by Δ = −0.0154(8) Å) in response to this initial onset of η^1-OSO photoisomer formation. The ruthenium-to-ligand nature of these photostructural changes indicates that η^1-OSO photoisomer formation is primarily responsible for the increase of a strong MLCT band in **1** during the first minute of light exposure, which we witness as the green-to-red waveband of light in Movies S1 and S2. This band assignment is also consistent with that of η^1-OSO formation in other [Ru−SO_2] complexes, $[Ru(SO_2)(NH_3)_4(H_2O)]$chlorobenzenesulfonate$_2$[24] and $[Ru(SO_2)(NH_3)_4$(3-bromopyridine)]tosylate$_2$.[25]

These Ru−$N_{pyridyl}$ and Ru−S_{dark} bond-length changes do not recover as **1** is subjected to further light exposure, which makes sense since they are directly associated with the η^1-OSO bond formation via a *trans* influence or the residual η^1-SO_2 species, respectively. Even larger, yet short-lived, bond-length increases (Δ = +0.0048(9)−0.0186(9) Å) are observed in the Ru−N_{ammine} coordination within the first minute of light exposure (Figure 5 (top left)). Similar, albeit more modest, spikes in bond lengths are witnessed at t = 1 min for most atoms in both cations and anions of **1**. The fluxional nature of these bond-length changes is presumably associated with the reorganiza-

https://doi.org/10.1021/acs.jpcc.1c04425
J. Phys. Chem. C 2021, 125, 15711−15723

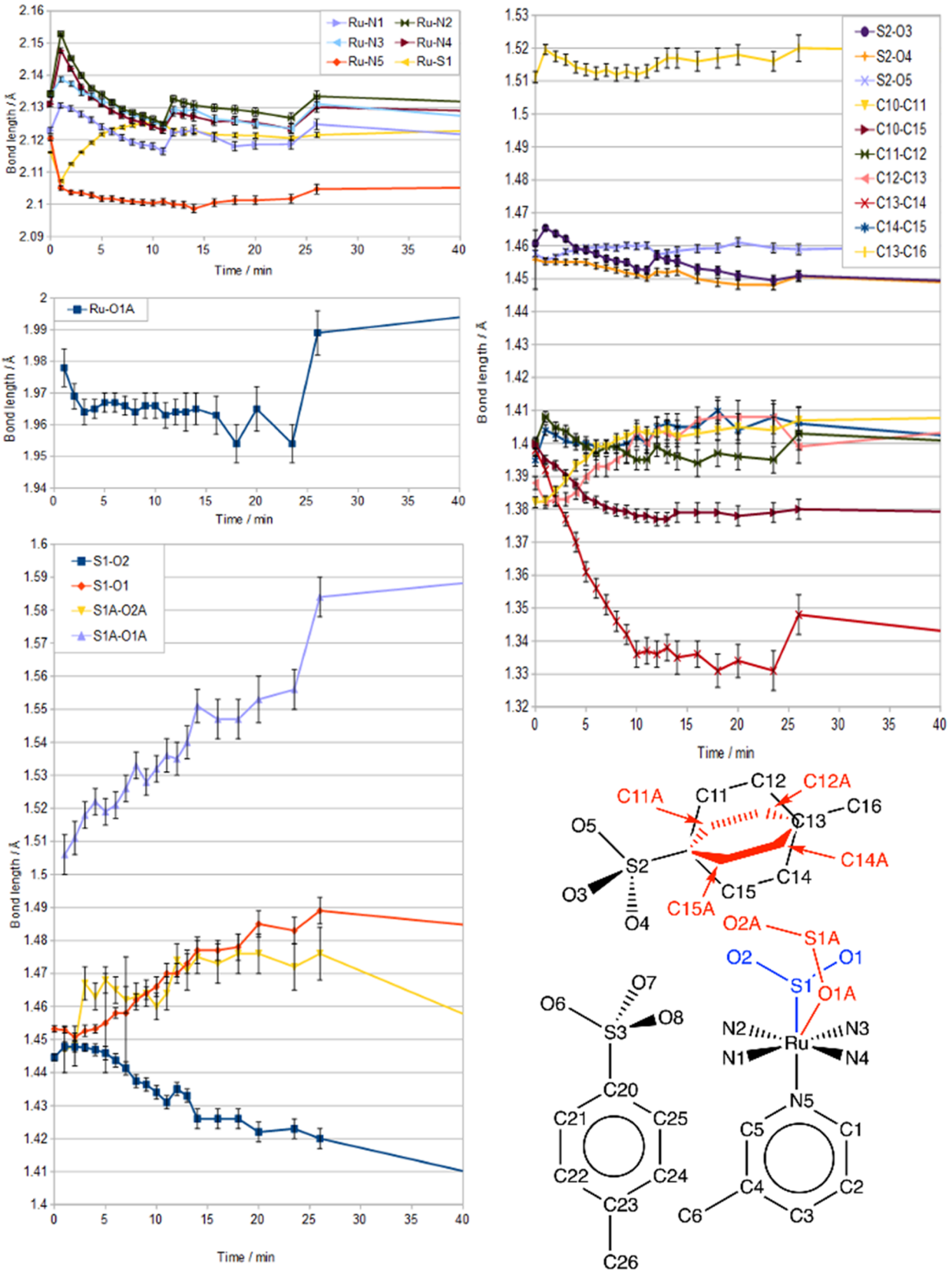

Figure 5. Bond-length changes in **1** as a function of light-exposure time, partitioned into distinct parts of the cation and anions: (top left) the ruthenium coordination environment; (bottom left) SO_2 isomers; and (top right) nondisordered part of the tosylate anion that exhibits rotational disorder.

tional energy that is needed to accommodate photoisomerization.

The Ru−O bond length in **1** at t = 1 min is 1.978(9) Å, which reduces to 1.964(4) Å over the next 2 min of light

https://doi.org/10.1021/acs.jpcc.1c04425
J. Phys. Chem. C 2021, 125, 15711−15723

exposure, thereafter remaining constant to time within experimental error up to t = 26.5 min (the onset of step 5, *vide infra*). This bond length converges rapidly, even though more cations in the crystal structure of **1** are photoisomerized with increasing light-exposure time. This suggests that the Ru−O bond is not further influenced by Ru in any significant fashion.

In contrast, the Ru−$N_{pyridyl}$ coordinative bond length in **1** continues to contract with increasing light-exposure duration, albeit more moderately after t = 1, until it levels out at about t = 10 min; see Figure 5 (top left). The extent by which this Ru−$N_{pyridyl}$ coordination in **1** is engaged in MLCT via π-back-bonding at any time, t, can be gauged from the bond-length differences, <Ru−N_{ammine} > −Ru−$N_{pyridyl}$.[51] This difference is 0.010(1) Å for t = 0 and 0.037(1) Å for t = 1 min, *i.e.*, 1 min of light exposure on **1** has the effect of increasing π-back-bonding in the Ru−$N_{pyridyl}$ coordinative bond by 0.027(1) Å. This corresponds to the maximum change in π-back-bonding seen at any time step in the light-exposure duration of **1** (see Figure S3, Supporting Information). This Ru−$N_{pyridyl}$ bond further contracts by 0.0034(8) Å during the period, $1 \leq t \leq 5$ min, wherein the aforementioned hypsochromic shift in the optical absorption of **1** starts to be observed (step 2, Figure 4).

Meanwhile, all four Ru−N_{ammine} bonds contract substantially within the time regime, $1 \leq t < 10$ min; their bond lengths cross through their original values by t = 5 min, after which point all Ru−N coordinative bonds undergo a net contraction relative to the dark-state configuration of **1**. Ru−O and Ru−$N_{pyridyl}$ are barely changing beyond t = 5 min. Meanwhile, a new peak starts to be resolvable in the optical absorption spectra of **1** at t = 5 min. All of these observations indicate that a new step in the operational mechanism of nanooptomechanical transduction in **1** onsets at t = 5 min (step 3, Figure 4).

This net bond contraction about the ruthenium core suggests that the significant Ru−N_{ammine} bond changes occur to account for some sort of charge effect. This effect is presumably correlated to the newly resolved optical absorption peak at t = 5 min, which continues to undergo a hypsochromic shift as it grows to reach a maximum optical absorbance at t = 10 min. Now, oxidation of the metal is unlikely to be a cause of this charge effect since Ru^{III}−N_{ammine} bond lengths are longer than those of Ru^{II}−N_{ammine} bonds in the related $[Ru(NH_3)_5(pyridine)]^{2+}$ ion.[51]

A more likely explanation is that this charge effect is, in some way, associated with one or more of the three other distinct structural changes that occur in **1** during the same time regime, $5 \leq t < 10$ min. The largest of these structural changes concern the ring rotor, whose photoconversion fraction increases maximally during this time period and levels off at t = 10 min of light-exposure duration. This is accompanied by substantial bond-length changes in the nondisordered component of the tosylate ion that involves the light-induced rotor, which occur up to t = 10 min (Figure 5 (top right)), especially for C13−C14 where Δ = −0.062(4) Å; C10−C15 also decreases monotonically by Δ = −0.022(2) Å. These changes are somewhat, but not wholly, compensated by bond-length expansions in C10−C11 and C12−C13. In contrast, while the nondisordered tosylate anion displays a holistically similar pattern of bond-length changes, they are far more modest and are largely zero within experimental error. Accordingly, only the tosylate ion that features the rotor may be related to the aforementioned charge effect in **1**. Another distinct structural change in **1** within the time regime, $5 \leq t <$ 10 min, is the ADP of C6: the methyl substituent of the pyridine ligand that neighbors this tosylate ion. This ADP increases by its maximal amount during this time duration (Figure 3, bottom right). Figures 1 and 2 show that this ADP is oblate whereby its maximal elongation points directly into the center of the ring rotor. Moreover, it would seem that one of the hydrogen atoms in this methyl group (H6A) participates in nonbonded interactions with the tosylate ion that features the rotor; *cf.* H6A−C11A = 2.440(2)−2.485(2) Å and H6A−C12A = 2.376(2)−2.406(2) Å at t = 5−10 min. More intense interactions that involve this ring rotor with a different pyridyl substituent have recently been observed in the related complex, $[Ru(SO_2)(NH_3)_4(3\text{-bromopyridine})]tosylate_2$.[25] Such interactions would provide a viable structural pathway that could link these two distinct structural changes involving the rotor to the Ru core via the pyridyl ring, thus offering an ICT channel that relates the Ru−N_{ammine} charge effect indirectly to the concomitant increase in arene ring rotation. Studies on ground-state structures have shown long-standing success in inferring ICT effects in optically active materials.[53−56] Nevertheless, further work is needed to confirm the precise nature of this charge effect; this will require a study in its own right. The other distinct structural change in **1** within the time regime, $5 \leq t < 10$ min, involves the continued η^1-OSO photoisomer formation, whose photoconversion fraction reaches a maximum at t = 10 min (see the pink line in top right, Figure 3); a compensatory depletion of the dark-state η^1-SO_2 isomer is demarcated by a continued increase in Ru−S bond lengths, which levels off at around t = 10 min (Figure 5 (top left)). The formation of this photoisomer is already known to be correlated to that of the rotor.[22]

Given all of these time-relevant structural correlations, the new peak that grows in the optical absorption spectra of **1** between t = 5 and 10 min (step 3, Figure 4) would thus appear to be due, at least in part, to a charge effect in these Ru−N_{ammine} net bond-length contractions, which are, in turn, related to the ring-rotor formation via some form of structurally connected pathway. This argument would also be consistent with the observation that this new optical absorption peak undergoes a hypsochromic shift (Figure 3) as this indicates structural changes, which cause disruption of ICT within a complex.

Meanwhile, the precise nature of the charge transfer that occurs within the immediate Ru core environment can be understood by considering that three of the Ru−N_{ammine} bond lengths are similar to each other, while the Ru−N1 bond length is disparate. Indeed, the geometrically opposing Ru−N1 and Ru−N3 bonds display a pseudo-Jahn−Teller effect throughout their light-exposure time profile (Figure 5 (top left)). Previous work on the closely related $[Ru(NH_3)_5(pyridine)]^{2+}$ ion[52] reported a similar pseudo-Jahn−Teller feature in the equatorial plane of its Ru−N_{ammine} bonds; this was attributed to a metal-centered (MC) charge transfer, and a substantial level of configurational mixing between MLCT and MC transitions was noted in this ion. Such mixing explained its lack of emissive characteristics. Likewise, **1** does not display any emission. It would thus seem reasonable to propose that MLCT and MC transitions in **1** from Ru−$N_{pyridyl}$ and Ru−N_{ammine} respectively, likewise undergo configurational mixing.

The Ru−N_{ammine} bond-length changes are much larger than those observed for the Ru−$N_{pyridyl}$ bond, and there are four of them compared to the one Ru−$N_{pyridyl}$ bond per cation. It is

https://doi.org/10.1021/acs.jpcc.1c04425
J. Phys. Chem. C 2021, 125, 15711−15723

therefore tempting to suggest that the newly resolved optical absorption peak is likely to be dominated by Ru−N_{ammine} MC charge transfer. However, it should be borne in mind that the Ru−$N_{pyridyl}$ MLCT transition exhibits an intense band in the closely related $[Ru(NH_3)_5(pyridine)]^{2+}$ ion, while the intensities of its MC transitions depend largely on the extent of MLCT and MC configurational mixing.[52]

The optical absorption peak in **1** starts to diminish at t = 11 min while continuing its hypsochromic shifting, and by t = 12 min, the Ru−$N_{pyridyl}$ bond stops contracting. All three bonds in the rotor whose lengths have contracted up to this point also stop changing suddenly at t = 12 min; this effect is particularly stark for the C13−C14 bond, while C10−C15 and C11−C12 carry the same trend, as shown in Figure 5 (top right). The cause of this sudden change at t = 12 min is illustrated via the Hirshfeld surfaces[57,58] of **1** for t = 11 and 12 min (Figure 6) and the nonbonded interactions shown in Table 1. The encircled regions of Figure 6 highlight the presence of close interactions between the methyl group of the 3-methylpyridine ligand and the disordered arene ring (shown in red), which shift suddenly between t = 11 and 12 min from one side of the arene ring to almost its center. The methyl group rotates during this period as it manages to move over the protruding edge of the disordered ring into a less strained configuration, as evidenced by a substantial change (Δ = +0.109(2)−0.112(2) Å) in its closest C_{methyl}−H···C_{arene} nonbonded interactions with the ring at t = 12 min; thereby, a different methyl hydrogen atom becomes the closest point of contact, as listed in Table 1. These light-induced interactions do not otherwise change significantly as a function of time, t. This is evidenced via the larger set of Hirshfeld surfaces shown in Figure S8, which map the start and end time points of all five distinct steps of the nanooptomechanical transduction operational mechanism in **1** (t = 0, 1, 5, 10, 11, 12, 26, 181 min).

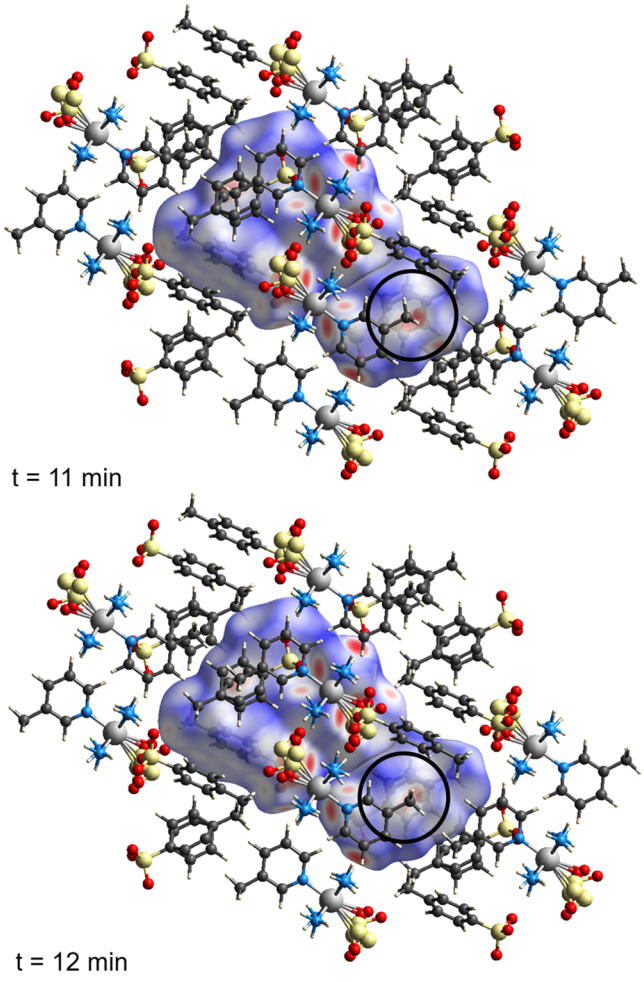

Figure 6. Hirshfeld surfaces of **1** after 11 and 12 min of light exposure, as viewed looking down the crystallographic a axis. The red, white, and blue regions show positive, neutral, and negative isoenergies. The encircled regions highlight a close nonbonded contact (in red) between the methyl group of the 3-methylpyridine ligand in **1** and its tosylate anion that exhibits a rotational disorder to alleviate the crystal-lattice strain that is caused by this close interaction. This methyl group rotates between t = 11 and 12 min of light exposure to lessen the strain; *cf.* the red area in the encircled region shifts to the center of the ring. Images were generated via CrystalExplorer.[58]

Rippling effects of this sudden structural change are manifested by corresponding, albeit more modest, jumps in bond lengths at t = 12 min that occur across the entire crystal lattice of **1** (Figures 5 and S2−S7). In particular, all four Ru−N_{ammine} bond lengths increase suddenly by 0.006(1) Å, on average, between t = 11 and 12 min, in response to this reconfiguration of cation···anion interactions. Thereafter, Ru−N1 and Ru−N3 bonds continue contracting again until t = 26 min, at which point another sudden jump in bond lengths is observed. Ru−N2 and Ru−N4 follow this same trend, except that their bond lengths level off for a short period between t = 12 and 14 min before they start to contract again. This leveling off brings the Ru−N_{ammine} bonds closer together, thereby yielding a smaller pseudo-Jahn−Teller effect, which we saw earlier was attributed to configurational mixing.[52] This observation suggests that the mixing of MLCT and MC charge-transfer states depletes during this period. Moreover, we noted earlier that such mixing is required to provide the MC bands from Ru−N_{ammine} bonding with good intensity,[52] while we observe a diminution of intensity in the optical absorption peak from 11 min < t < 26 min (step 4, Figure 4). This peak continues to shift hypsochromatically during this period, in line with the continuing Ru−N_{ammine} bond-length contractions until t = 26 min, at which point it can no longer be resolved from the broader envelope of optical absorption.

Meanwhile, the photoconversion fraction of the rotor levels off during this time range of step 4 (Figure 3). The η^1-OSO photoconversion fraction also decreases a little during this time, which results in a commensurate increase in the photoconversion fraction of the η^1-SO_2 dark-state configuration (top right, Figure 3). The associated Ru−S1 bond length contracts, as seen in Figure 5 (top left), which will also alleviate some of the need for the Ru−N bonds to contract.

We mentioned that a second sudden jump occurs in most bond lengths of **1** at t = 26 min, as shown in Figures 5 and S2−S7. This jump appears to be due to interactions between the SO_2 group and the rotor, which reach a limit at t = 26 min. As stated earlier (Scheme 1), the basic operational mechanism of nanooptomechanical transduction in $[RuSO_2]$ complexes deduced by Sylvester and Cole[22] involves such interactions. Thereby, the oxygen that protrudes from the η^1-OSO photoisomer lies very close to a hydrogen of the nondisordered part of the disordered arene ring, yielding crystal-lattice strain. This strain becomes too great to sustain, as the photoconversion fraction of η^1-OSO photoisomers reaches a certain level; in response, it relaxes by the process of rotational

https://doi.org/10.1021/acs.jpcc.1c04425
J. Phys. Chem. C 2021, 125, 15711−15723

Table 1. Nonbonded Contacts and Extent of Ring Rotation in 1 as a Function of Light-Exposure Time at the Start and End Time Points of Each of the Five Discrete Steps of the Operational Mechanism for Nanooptomechanical Transduction[a]

time, t (min)	ring rotation (deg)	C6−H6A/C··· C11/A length (Å)	C6−H6A/C···C12/A length (Å)
0		C6−H6A···C11: 3.055(3)	C6−H6A···C12: 2.746(3)
1	46.2(2)	C6−H6A···C11A: 2.37(3)	C6−H6A···C12A: 2.35(3)
5	47.3(7)	C6−H6A···C11A: 2.440(2)	C6−H6A···C12A: 2.376(2)
10	48.7(4)	C6−H6A···C11A: 2.485(2)	C6−H6A···C12A: 2.406(2)
11	48.6(7)	C6−H6**A**···C11A: **2.496(2)**	C6−H6**A**···C12A: **2.414(2)**
12	48.8(7)	C6−H6**C**···C11A: **2.608(2)**	C6−H6**C**···C12A: **2.523**(2)
26	50.0(11)	C6−H6C···C11A: 2.633(3)	C6−H6C···C12A: 2.527(3)
181	51.4(11)	C6−H6C···C11A: 2.64(3)	C6−H6C···C12A: 2.56(3)

[a]The emboldened values highlight the key changes that are observed between t = 11 and 12 min of light-exposure time.

disorder such that the rotor forms. The same process can be seen in **1**, whereby O2A is the protruding oxygen to which the hydrogen, H15A, lies particularly close, as shown in Figure 7.

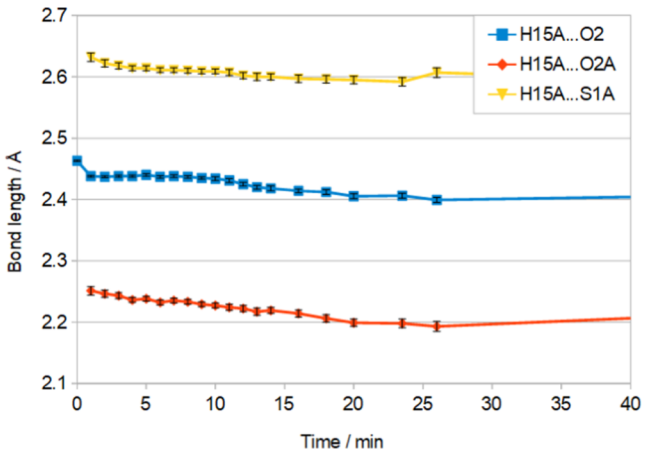

Figure 7. Changes in lengths of the nonbonded contacts, C15−H15A···O2, C15−H15A···O2A, and C15−H15A···S1A in **1** as a function of light-exposure time, which denote the interactions between the η^1-OSO and η^1-SO_2 isomers of **1** and a hydrogen of the nondisordered part of the arene ring of the tosylate anion that contains the rotor. These interactions contract to a converging limit at t = 26 min.

This plot also reveals that H15A lies close to the adjoining sulfur, S1A, of the η^1-OSO photoisomer, as well as one of the dark-state oxygen atoms, O2. Figure 7 evidences that all three interactions decrease with increasing light-exposure time until t = 26 min, whereby the length of these nonbonded contacts appears to converge to a limit. A steep jump in an already increasing S1A−O1A bond length is observed at this point, as shown in Figure 5 (bottom left). The Ru−O bond length increases by a similar amount at t = 26 min, despite being pretty unresponsive to light exposure otherwise. This would suggest that O1A is bound tightly to the Ru ion, such that the S1A−O1A bond takes up the slack until t = 26 min when the crystal-lattice strain becomes too great for the H15A···O2A bond to be able to further contract. Both Ru−O and S1A−O1A bonds suddenly lengthen considerably in response. The resulting S1A−O1A bond length (1.584(6) Å at t = 26 min; 1.599(9) Å at t = 181 min once fully light saturated) represents the longest reported S−O bond in any metal-bound η^1-OSO ligand, as evidenced by the Cambridge Structural Database;[59] hitherto, the longest such bond ever reported belongs to the closely related $[Ru(SO_2)(NH_3)_4(3\text{-phenylpyridine})]Cl_2{\cdot}H_2O$ complex whose S−O−(Ru) bond length is 1.566 Å.[26] There is a considerable knock-on effect in most of the other bond lengths in **1**, presumably because the sudden Ru−O bond-length change will perturb the metal-based charge transfer of the cation and thus the charge of all ions in **1**.

This step change in bond lengths also coincides with a slight depletion in the minor photoisomeric species, η^2-(OS)O, whose photoconversion fraction becomes too low for its oxygen atoms to be modeled. This depletion of the η^2-(OS)O photoisomer could explain the formation of the dip in the 425−474 nm region of the optical absorption spectrum for **1** that appears at t = 26 min.

The operational mechanism of nanooptomechanical transduction enters its final phase (step 5, Figure 4) at t = 26 min. Beyond this time frame, the optical absorption profile undergoes a slight increase in its long-wavelength peak, which we saw earlier is associated with an increase in the η^1-OSO photoconversion fraction. The photostructural changes in the time frame 26 ≤ t ≤ 181 min show a correspondingly marginal increase in the η^1-OSO photoisomer formation, while other structural changes converge to a steady metastable state (see Figures S8−S13). Most atoms in **1** also appear to absorb light as heat after t = 40 min, judging from their increase in ADP values with this concomitant increase in long-wavelength absorption. Meanwhile, U_{11} of C6 is particularly large and reaches its maximum value during this step (Figure 3, bottom right). This presumably relates to our earlier observation that this methyl group participates in nonbonded interactions with the rotor, while the extent of disorder in this ring is barely changing at this point.

Mechanistic Interpretation of Nanooptomechanical Transduction in 1. Considering all of the above observations and metal-based charge-transfer assignments, the overall stepwise mechanism of nanooptomechanical transduction in **1** can be interpreted as follows. (Step 1, 5 s ≤ t ≤ 1 min): η^1-OSO photoisomer formation with the corresponding increase in an intense MLCT band between 550 and 750 nm that is due to π-back-bonding in the Ru−$N_{pyridyl}$ bond. (Step 2, 1 ≤ t ≤ 5 min): Ru−N_{ammine} bond lengths return to their dark-state values as the light-induced crystal structure adapts to the photoisomerization process. The Ru−N_{ammine} and Ru−$N_{pyridyl}$ bonds are associated with the onset of a hypsochromic shift. The fractions of each photoconverted species start to become correlated. (Step 3, 5 ≤ t ≤ 10 min): all Ru−N bonds in the cation of **1** undergo a net contraction; this charge effect seems to be related indirectly to the tosylate anion whose arene ring displays a rotational disorder. The continuing Ru−N_{ammine} bond contractions engender a newly resolved hypsochromically shifting peak in the optical absorption spectrum; this represents MC charge transfer, which is configurationally

https://doi.org/10.1021/acs.jpcc.1c04425
J. Phys. Chem. C 2021, 125, 15711−15723

mixed with the MLCT that occurs due to Ru−$N_{pyridyl}$ π-back-bonding. The photoinduced structural changes in the cations and anions of **1** are now highly correlated as the nano-optomechanical transduction becomes pronounced. (Step 4, $11 \leq t \leq 26$ min): the Ru−N_{ammine} bonds further contract, although the configurational mixing of its MC charge transfer with MLCT declines. This causes the new peak in the optical absorption spectrum of **1** to start to diminish at t = 11 min, having reached its maximum at t = 10 min; it continues to shift hypsochromatically while it depletes eventually to the point where it can no longer be resolved from the underpinning broad envelope of the optical absorption spectrum. The photoconversion fraction of the rotational disorder in the ring rotor levels off during this time frame; the η^1-OSO photo-isomer also decreases a little during this step. Meanwhile, a sudden change in most bond lengths is noticed at t = 12 min. The cause is the methyl group of the 3-methylpyridine ligand in **1**, which structurally reconfigures to alleviate the crystal-lattice strain that has built up between one of its hydrogen atoms and the photoinduced rotational disorder in the arene ring of the rotor. The rest of the crystal structure of **1** responds by most of its bond lengths undergoing a sudden change at t = 12 min. (Step 5, $26 \leq t \leq 181$ min): another sudden jump in bond lengths is witnessed in most bonds of **1** at t = 26 min. This is primarily caused by interactions between the η^1-OSO photoisomer and an arene-ring hydrogen in the tosylate ion, which undergoes a disorder to alleviate the crystal-lattice strain that has built up to a critical point at this time. This affects the metal-based charge transfer in the ruthenium ion, which in turn affects most bond lengths in **1** owing to its effect on charge. A slight depletion of the minor η^2-(OS)O photo-isomeric species is also observed at this time; a corresponding dip in the optical absorption spectrum starts to be observed in the region of 425−475 nm. Thereafter, **1** absorbs light as heat as witnessed by the increasing ADPs of most of its atoms. Meanwhile, the η^1-OSO photoisomer increases slightly as all structural changes converge toward a steady metastable state.

CONCLUSIONS

In summary, a molecular movie has permitted the mechanism of nanooptomechanical transduction in the newly discovered single-crystal optical actuator, **1**, to be unraveled. The correlated rendering of its structural and optical absorption properties has facilitated the assignments of MLCT and MCCT bands in **1**, which increase and decrease in correspondence with the photostructural changes that unfold during this optical actuation process. We have shown that the originally cast basic operational mechanism for nanooptome-chanical transduction that occurs in certain [$RuSO_2$] complexes is also mirrored in this study of **1**. However, the overall mechanism is far more complicated than originally envisaged; it appears to occur via five discrete mechanistic steps that involve complex and correlated optical and structural effects. These detailed mechanistic insights that have been afforded by this work will assist in the molecular design of new nanooptomechanical transducers in [$RuSO_2$] compounds, as well as help to characterize the fundamental optical and structural properties of SO_2 linkage photoisomerization in coordination chemistry. In broader terms, our demonstrated ability to assign metal-based charge-transfer bands in single-crystal optical absorption spectra directly from light-induced crystal structures could be useful in all manner of optoelectronic processes.

ASSOCIATED CONTENT

Supporting Information

The Supporting Information is available free of charge at https://pubs.acs.org/doi/10.1021/acs.jpcc.1c04425.

Material synthesis and characterization methods for **1**; photochromism of **1** as a function of light-exposure time, as viewed by single-crystal optical absorption microscopy; bond-length changes in **1** as a function of light-exposure time; Hirshfeld surfaces of **1** as a function of light-exposure time; crystallographic information files (CIFs) of the dark-state crystal structure of **1** and its 12 and 23 light-induced crystal structures that were collected on crystals I and II as a function of light-exposure time from t = 0 to 120 s and t = 0 to 181 min, respectively (PDF)

Changes in the crystal structure and optical absorption spectrum of **1** as a function of light-exposure time for crystal I (Movie S1) (MP4)

Changes in the crystal structure and optical absorption spectrum of**1** as a function of light-exposure time for crystal II (Movie S2) (MP4)

AUTHOR INFORMATION

Corresponding Author

Jacqueline M. Cole − *Cavendish Laboratory, Department of Physics, University of Cambridge, Cambridge CB3 0HE, U.K.; ISIS Neutron and Muon Source, STFC Rutherford Appleton Laboratory, Didcot OX11 0QX, U.K.; Department of Chemical Engineering and Biotechnology, University of Cambridge, Cambridge CB3 0AS, U.K.; Argonne National Laboratory, Argonne, Illinois 60439, United States;* orcid.org/0000-0002-1552-8743; Email: jmc61@cam.ac.uk

Authors

David J. Gosztola − *Argonne National Laboratory, Argonne, Illinois 60439, United States;* orcid.org/0000-0003-2674-1379

Sven O. Sylvester − *Cavendish Laboratory, Department of Physics, University of Cambridge, Cambridge CB3 0HE, U.K.*

SuYin Grass Wang − *NSF's ChemMatCARS Beamline, The University of Chicago, Argonne, Illinois 60439, United States;* orcid.org/0000-0001-8474-9817

Yu-Sheng Chen − *NSF's ChemMatCARS Beamline, The University of Chicago, Argonne, Illinois 60439, United States*

Complete contact information is available at: https://pubs.acs.org/10.1021/acs.jpcc.1c04425

Notes

The authors declare no competing financial interest.

ACKNOWLEDGMENTS

J.M.C. is grateful for the BASF/Royal Academy of Engineering Research Chair in the Data-Driven Molecular Engineering of Functional Materials, which is partly supported by the STFC via the ISIS Neutron and Muon Source. J.M.C. also thanks the 1851 Royal Commission of the Great Exhibition for the 2014 Fellowship in Design, hosted by Argonne National Laboratory where the work done was supported by the U.S. Department of Energy (DOE) Office of Science, Office of Basic Energy Sciences, and used research resources of the Center for Nanoscale Materials and the Advanced Photon Source, Office

of Science User Facilities operated for the DOE Office of Science by Argonne National Laboratory, supported by the U.S. DOE, all under contract no. DE-AC02-06CH11357. NSF's ChemMatCARS Sector 15 is supported by the Divisions of Chemistry (CHE) and Materials Research (DMR), National Science Foundation, under grant number NSF/CHE-1834750. S.O.S. acknowledges the Cambridge Commonwealth Trust for a Ph.D. Scholarship.

REFERENCES

(1) Refaely-Abramson, S.; Jain, M.; Sharifzadeh, S.; Neaton, J. B.; Kronik, L. Solid-state optical absorption from optimally tuned time-dependent range-separated hybrid density functional theory. *Phys. Rev. B* **2015**, *92*, No. 081204.

(2) Coppens, P.; Fomitchev, D. V.; Carducci, M. D.; Culp, K. Crystallography of molecular excited states. Transition-metal nitrosyl complexes and the study of transient species. *J. Chem. Soc., Dalton Trans.* **1998**, *6*, 865−872.

(3) Cole, J. M. Single-crystal X-ray diffraction studies of photo-induced molecular species. *Chem. Soc. Rev.* **2004**, *33*, 501−513.

(4) Cole, J. M. Photocrystallography. *Acta Crystallogr., Sect. A: Found. Crystallogr.* **2008**, *64*, 259−271.

(5) Cole, J. M. A new form of analytical chemistry: distinguishing the molecular structure of photo-induced states from ground-states. *Analyst* **2011**, *136*, 448−455.

(6) Cole, J. M. Applications of photocrystallography: a future perspective. *Z. Kristallogr.* **2008**, *223*, 363−369.

(7) Cole, J. M.; Gosztola, D. J.; Velazquez-Garcia, J. dJ.; Chen, Y-S. Systems Approach of Photoisomerization Metrology for Single-Crystal Optical Actuators: A Case Study of $[Ru(SO_2)(NH_3)_4Cl]Cl$. *J. Phys. Chem. C* **2020**, *124*, 28230−28243.

(8) Masciocchi, N.; Kolyshev, A. N.; Dulepov, V. E.; Boldyreva, E. V.; Sironi, A. Study of the Linkage Isomerization $[Co(NH_3)_5NO_2]Br_2 \leftrightarrow [Co(NH_3)_5ONO]Br_2$ in the Solid State by X-ray Powder Diffraction. *Inorg. Chem.* **1994**, *33*, 2579−2585.

(9) Hatcher, L. E.; Skelton, J. M.; Warren, M. R.; Raithby, P. R. Photocrystallographic Studies on Transition Metal Nitrito Metastable Linkage Isomers: Manipulating the Metastable State. *Acc. Chem. Res.* **2019**, *52*, 1079−1088.

(10) Hatcher, L. E.; Warren, M. R.; Allan, D. R.; Brayshaw, S. K.; Johnson, A. L.; Fuertes, S.; Schiffers, S.; Stevenson, A. J.; Teat, S. J.; Woodall, C. H.; et al. Metastable Linkage Isomerism in $[Ni(Et_4dien)(NO_2)_2]$: A Combined Thermal and Photocrystallographic Structural Investigation of a Nitro/Nitrito Interconversion. *Angew. Chem., Int. Ed.* **2011**, *50*, 8371−8374.

(11) Hatcher, L. E. Raising the (metastable) bar: 100% photo-switching in $[Pd(Bu_4dien)(\eta^1\text{-}NO_2)]^+$ approaches ambient temperature. *Cryst. Eng. Commun.* **2016**, *18*, 4180−4187.

(12) Schaniel, D.; Imlau, M.; Weismoeller, M.; Woike, T.; Kraemer, K.; Guedel, H. U. Photoinduced Nitrosyl Linkage Isomers Uncover a Variety of Unconventional Photorefractive Media. *Adv. Mater.* **2007**, *19*, 723−726.

(13) Cormary, B.; Ladeira, S.; Jacob, K.; Lacroix, P.; Woike, T.; Schaniel, D.; Malfant, I. Structural Influence on the Photochromic Response of a Series of Ruthenium Mononitrosyl Complexes. *Inorg. Chem.* **2012**, *51*, 7492−7501.

(14) Fomitchev, D. V.; Bagley, K. A.; Coppens, P. The First Crystallographic Evidence for Side-On Coordination of N_2 to a Single Metal Center in a Photoinduced Metastable State. *J. Am. Chem. Soc.* **2000**, *122*, 532−533.

(15) Cheng, L.; Novozhilova, I.; Kim, C. D.; Kovalevsky, A.; Bagley, K. A.; Coppens, P.; Richter-Addo, G. B. First Observation of Photoinduced Nitrosyl Linkage Isomers of Iron Nitrosyl Porphyrins. *J. Am. Chem. Soc.* **2000**, *122*, 7142−7143.

(16) Powers, D. C.; Anderson, B. L.; Hwang, S. J.; Powers, T. M.; Perez, L. M.; Hall, M. B.; Zheng, S-L.; Chen, Y-S.; Nocera, D. G. Photocrystallographic Observation of Halide-Bridged Intermediates in Halogen Photoeliminations. *J. Am. Chem. Soc.* **2014**, *136*, 15346−15355.

(17) Sun, J.; Abbenseth, J.; Verplancke, H.; Diefenbach, M.; de Bruin, B.; Hunger, D.; Wuertele, C.; van Slageren, J.; Holthausen, M. C.; Schneider, S. A Platinum(II) Metallonitrene with a Triplet Ground State. *Nat. Chem.* **2020**, *12*, 1054−1059.

(18) Das, A.; Reibenspies, J. H.; Chen, Y-S.; Powers, D. C. Direct Characterization of a Reactive Lattice-confined Ru_2 Nitride by Photocrystallography. *J. Am. Chem. Soc.* **2017**, *139*, 2912−2915.

(19) Kovalevsky, A. Yu.; Bagley, K. A.; Coppens, P. The First Photocrystallographic Evidence for Light-Induced Metastable Linkage Isomers of Ruthenium Sulfur Dioxide Complexes. *J. Am. Chem. Soc.* **2002**, *124*, 9241−9248.

(20) Kovalevsky, A. Yu.; Bagley, K. A.; Cole, J. M.; Coppens, P. Light-Induced Metastable Linkage Isomers of Ruthenium Sulfur Dioxide Complexes. *Inorg. Chem.* **2003**, *42*, 140−147.

(21) Bowes, K. F.; Cole, J. M.; Husheer, S. L. G.; Raithby, P. R.; Savarese, T.; Sparkes, H. A.; Teat, S. J.; Warren, J. E. Photocrystallographic structure determination of a new geometric isomer of $[Ru(NH_3)_4(H_2O)(\eta^1\text{-}OSO)][MeC_6H_4SO_3]_2$. *Chem. Commun.* **2006**, 2448−2450.

(22) Sylvester, S. O.; Cole, J. M. Solar-Powered Nanomechanical Transduction from Crystalline Molecular Rotors. *Adv. Mater.* **2013**, *25*, 3324−3328.

(23) Sylvester, S. O.; Cole, J. M.; Waddell, P. G.; Nowell, H.; Wilson, C. SO_2 Phototriggered Crystalline Nanomechanical Transduction of Aromatic Rotors in Tosylates: Rationalization via Photocrystallography of $[Ru(NH_3)_4SO_2X]$tosylate$_2$ (X = pyridine, 3-Cl-pyridine, 4-Cl-pyridine). *J. Phys. Chem. C* **2014**, *118*, 16003−16010.

(24) Cole, J. M.; Gosztola, D. J.; Velazquez-Garcia, J. d. J.; Wang, S. G.; Chen, Y-S. Rapid Build Up of Nanooptomechanical Transduction in Single Crystals of a Ruthenium-based SO_2 Linkage Photoisomer. *Chem. Commun.* **2021**, *57*, 1320−1323.

(25) Cole, J. M.; Gosztola, D. J.; Velazquez-Garcia, J. d. J. Nanooptomechanical Transduction in a Single Crystal with 100% Photoconversion. *J. Phys. Chem. C* **2021**, *125*, 8907−8915.

(26) Cole, J. M.; Velazquez-Garcia, J. J.; Gosztola, D. J.; Wang, S.-Y. G.; Chen, Y.-S. Light-Induced Macroscopic Peeling of Single-Crystal Driven by Photoisomeric Nano-Optical Switching. *Chem. Mater.* **2019**, *31*, 4927−4935.

(27) Sylvester, S. O.; Cole, J. M. Quantifying Crystallographically Independent Optical Switching Dynamics in Ru SO_2 Photoisomers via Lock-and-Key Crystalline Environment. *J. Phys. Chem. Lett.* **2013**, *4*, 3221−3226.

(28) Sylvester, S. O.; Cole, J. M.; Waddell, P. G. Photoconversion Bonding Mechanism in Ruthenium Sulfur Dioxide Linkage Photoisomers Revealed by in Situ Diffraction. *J. Am. Chem. Soc.* **2012**, *134*, 11860−11863.

(29) Cole, J. M.; Velazquez-Garcia, J. J.; Gosztola, D. J.; Wang, S. G.; Chen, Y.-S. η^2-SO_2 Linkage Photoisomer of an Osmium Coordination Complex. *Inorg. Chem.* **2018**, *57*, 2673−2677.

(30) Phillips, A. E.; Cole, J. M.; d'Almeida, T.; Low, K. S. Ru−OSO Coordination Photogenerated at 100 K in Tetraammineaqua(sulfur dioxide)ruthenium(II) (±)-Camphorsulfonate. *Inorg. Chem.* **2012**, *51*, 1204−1206.

(31) Phillips, A. E.; Cole, J. M.; d'Almeida, T.; Low, K. S. Effects of the reaction cavity on metastable optical excitation in ruthenium-sulfur dioxide complexes. *Phys. Rev. B* **2010**, *82*, No. 155118.

(32) Cole, J. M.; Gosztola, D. J.; Sylvester, S. O. Low-energy Optical Switching of SO_2 Linkage Isomerization in Single Crystals of a Ruthenium-based Coordination Complex. *RSC Adv.* **2021**, *11*, 13183−13192.

(33) Naumov, P.; Karothu, D. P.; Ahmed, E.; Catalano, L.; Commins, P.; Halabi, J. M.; Al-Handawi, M. B.; Li, L. The Rise of the Dynamic Crystals. *J. Am. Chem. Soc.* **2020**, *142*, 13256−13272.

(34) Naumov, P.; Chizhik, S.; Panda, M. K.; Nath, N. K.; Boldyreva, E. Mechanically Responsive Molecular Crystals. *Chem. Rev.* **2015**, *115*, 12440−12490.

https://doi.org/10.1021/acs.jpcc.1c04425
J. Phys. Chem. C 2021, 125, 15711−15723

(35) Abendroth, J. M.; Bushuyev, O. S.; Weiss, P. S.; Barrett, C. J. Controlling Motion at the Nanoscale: Rise of the Molecular Machines. *ACS Nano* **2015**, *9*, 7746−7768.
(36) Tong, F.; Xu, W.; Guo, T.; Lui, B. F.; Hayward, R. C.; Palffy-Muhoray, P.; Al-Kaysi, R. O.; Bardeen, C. J. Photomechanical molecular crystals and nanowire assemblies based on the [2+2] photodimerization of a phenylbutadiene derivative. *J. Mater. Chem. C* **2020**, *8*, 5036−5044.
(37) Al-Kaysi, R. O.; Tong, F.; Al-Haidar, M.; Zhu, L.; Bardeen, C. J. Highly branched photomechanical crystals. *Chem. Commun.* **2017**, *53*, 2622−2625.
(38) Liu, T.; Pagliano, F.; van Veldhoven, R.; Pogoretskiy, V.; Jiao, Y.; Fiore, A. Integrated nano-optomechanical displacement sensor with ultrawide optical bandwidth. *Nat. Commun.* **2020**, *11*, No. 2407.
(39) Wang, J.; Feringa, B. L. Dynamic Control of Chiral Space in a Catalytic Asymmetric Reaction Using a Molecular Motor. *Science* **2011**, *331*, 1429−1432.
(40) Koumura, N.; Zijlstra, R.; van Delden, R.; Harada, N.; Feringa, B. L. Light-driven monodirectional molecular rotor. *Nature* **1999**, *401*, 152−155.
(41) Bochmann, J.; Vainsencher, A.; Awschalom, D. D.; Cleland, A. N. Nanomechanical coupling between microwave and optical photons. *Nat. Phys.* **2013**, *9*, 712−716.
(42) Coskun, A.; Banaszak, M.; Astumian, R. D.; Stoddart, J. F.; Grzybowski, B. A. Great expectations: can artificial molecular machines deliver on their promise? *Chem. Soc. Rev.* **2012**, *41*, 19−30.
(43) Mukaddem, K. T.; Cole, J. M.; Beyer, K. A.; Sylvester, S. O. Local Atomic Structure in Photoisomerized Ruthenium Sulfur Dioxide Complexes Revealed by Pair Distribution Function Analysis. *J. Phys. Chem. C* **2020**, *124*, 10094−10104.
(44) Phillips, A. E.; Cole, J. M.; Low, K. S.; Cibin, G. $L_{2,3}$-edge x-ray absorption near-edge spectroscopy analysis of photoisomerism in solid ruthenium−sulfur dioxide complexes. *J. Phys.: Condens. Matter* **2013**, *25*, No. 085505.
(45) Dolomanov, O. V.; Bourhis, L. J.; Gildea, R. J.; Howard, J. A. K.; Puschmann, H. OLEX2: a complete structure solution, refinement and analysis program. *J. Appl. Crystallogr.* **2009**, *42*, 339−341.
(46) Duyens, L. N. M. The flattening of the absorption spectrum of suspensions, as compared to that of solutions. *Biochim. Biophys. Acta* **1956**, *19*, 1−12.
(47) Corbett, D.; Warner, M. Linear and Nonlinear Photoinduced Deformations of Cantilevers. *Phys. Rev. Lett.* **2007**, *99*, No. 174302.
(48) Corbett, D.; Warner, M. Bleaching and stimulated recovery of dyes and of photocantilevers. *Phys. Rev. E* **2008**, *77*, No. 051710.
(49) Ichimura, K. Isosbestic Points do not Always Work as a Measure to Determine the Oneness of a Reaction as Exemplified by the Photoisomerization of Azobenzene Tethered to Polymer Chains. *Chem. Lett.* **2018**, *47*, 1247−1250.
(50) Mews, R.; Lork, E.; Watson, P. G.; Goertler, B. Coordination chemistry in and of sulfur dioxide. *Coord. Chem. Rev.* **2000**, *197*, 277−320.
(51) Shin, Y. K.; Szalda, D. J.; Brunschwig, B. S.; Creutz, C.; Sutin, N. Electronic and Molecular Structures of Pentaammineruthenium Pyridine and Benzonitrile Complexes as a Function of Oxidation State. *Inorg. Chem.* **1997**, *36*, 3190−3197.
(52) Tsai, C. N.; Mazumder, S.; Zhang, X. Z.; Schlegel, H. B.; Chen, Y. J.; Endicott, J. F. Metal-to-ligand Charge-Transfer Emissions of Ruthenium(II) Pentaammine Complexes with Monodentate Aromatic Acceptor Ligands and Distortion Patterns of their Lowest Energy Triplet Excited States. *Inorg. Chem.* **2015**, *54*, 8495−8508.
(53) Marder, S. R.; Gorman, C. B.; Tiemann, B. G.; Perry, J. W.; Bourhill, G.; Mansour, K. Relation Between Bond-Length Alternation and Second Electronic Hyperpolarizability of Conjugated Organic Molecules. *Science* **1993**, *261*, 186−189.
(54) Cheng, L. T.; Tam, W.; Stevenson, S. H.; Meredith, G. R.; Rikken, G.; Marder, S. R. Experimental investigations of organic molecular nonlinear optical polarizabilities. 1. Methods and results on benzene and stilbene derivatives. *J. Phys. Chem. A* **1991**, *95*, 10631−10643.
(55) Cheng, L. T.; Tam, W.; Marder, S. R.; Stiegman, A. E.; Rikken, G.; Spangler, C. W. Experimental investigations of organic molecular nonlinear optical polarizabilities. 2. A study of conjugation dependences. *J. Phys. Chem. B* **1991**, *95*, 10643−10652.
(56) Cole, J. M. Organic materials for second-harmonic generation: advances in relating structure to function. *Philos. Trans. R. Soc. London, Ser. A* **2003**, *361*, 2751−2770.
(57) Spackman, M. A.; Byrom, P. G. A novel definition of a molecule in a crystal. *Chem. Phys. Lett.* **1997**, *267*, 215−220.
(58) Turner, M. J.; McKinnon, J. J.; Wolff, S. K.; Grimwood, D. J.; Spackman, P. R.; Jayatilaka, D.; Spackman, M. A. *CrystalExplorer*, version 17; University of Western Australia: Perth, WA, Australia, 2017.
(59) Groom, C. R.; Bruno, I. J.; Lightfoot, M. P.; Ward, S. C. The Cambridge Structural Database. *Acta Crystallogr., Sect. B: Struct. Sci., Cryst. Eng. Mater.* **2016**, *72*, 171−179.

https://doi.org/10.1021/acs.jpcc.1c04425
J. Phys. Chem. C 2021, 125, 15711−15723